Identifying and overcoming deficiencies of nuclear data on the fission of light actinides by use of the GEF code

Karl-Heinz Schmidt, Christelle Schmitt, Andreas Heinz, Beatriz Jurado

Identifying and overcoming deficiencies of nuclear data on the fission of light actinides by use of the GEF code

Karl-Heinz Schmidt (1), Christelle Schmitt (2), Andreas Heinz(3), Beatriz Jurado (4)
((1) Rheinstr. 4, 64390 Erzhausen, Germany
(2) Institut Pluridisciplinaire Hubert Curien, CNRS/IN2P3-UDS, 67037 Strasbourg Cedex 2, France,
(3) Department of Physics, Chalmers University of Technology, 41296 Gothenburg, Sweden,
(4) Université de Bordeaux, CNRS, LP2I, Bordeaux, 33170, Gradignan, France)

Fission of light actinides has shown to exhibit features which abruptly deviate from the monotonous trend established for heavier systems. More specifically, the description of their fission excitation functions and fragment angular anisotropies was found impossible to reconcile with the statistical-model framework employing a double-humped fission barrier profile, which was successfully applied to heavy nuclei. This was referred to as the “thorium anomaly” in the 1970’s, and was interpreted in terms of the occurrence of a triple-humped barrier. Over the years, its impact on other fission quantities, in particular on the fission yields, has nevertheless been overlooked. In this work we show the drastic influence of the third barrier on the fission-fragment mass (equivalently, charge) and total kinetic energy at excitation energies close to the barrier. The analysis of these observables, and of their variation as a function of initial excitation energy, reveals the suppression of compact (and possibly very elongated) shapes at scission in light actinides. An extension of the semi- empirical GEF code [K.-H. Schmidt et al., Nucl. Data Sheets 131 (2016) 107] is developed that relates this suppression to the influence of the third barrier. Accounting for this specific feature of light actinides is crucial for a proper description of the fission of the nuclides involved in ^{235}U-driven reactors, and, to a higher degree, those of the Th-U cycle. These features are not considered in present official nuclear-data tables. Systematic fragment-yield predictions are provided.

Layout

1. Introduction

Since its discovery in the late 1930's [1] , nuclear fission has been extensively studied, due to its significance for both fundamental physics as well as for its role in various societal applications. While a certain level of understanding has been reached with several general trends and systematics, which are now well established, a comprehensive picture is still missing. This is in particular true for fissioning nuclei in specific areas of the nuclear chart, even though those can have a substantial impact on both the fundamental and applied domains.

For the design and for the operation of nuclear power plants, a good knowledge of the relevant nuclear data is mandatory. This includes the yields of the fragments, produced in the fission of the nuclear species that are present in the fuel induced by neutrons of different energies E_n, the fragment kinetic energies, the multiplicities and the spectra of the prompt and delayed post-scission neutrons as well as the properties of the prompt and delayed gammas. In the past, great effort has been invested in measuring these data with different methods as complete and as accurate as possible.

The early experiments were focused on the needs of the Manhattan project [2] and on the simulation of nuclear power plants that are based on the fission of ^{235}U. They were performed with large effort. However, the experimental knowledge on fragment yields is still very much limited: Even the most comprehensive evaluations [3] only cover fission induced by thermal, fast (energy E_n around 0.5 MeV) and $E_n \approx$ 14-MeV neutrons of a handfull of target nuclei.

It is known that thorium-based nuclear power generation, which is fueled primarily by the fission of the isotope ^{233}U produced from the fertile element thorium, has important advantages [4]. It is currently envisaged as a viable alternative to fossile combustibles [4,5], and a demonstrator of a molten-salt reactor, which uses thorium as a fuel, has been built [6]. This means that the data on the fission of the nuclides ^{230}Th, ^{231}Pa, ^{233}Pa, ^{234}U and ^{236}U, the key nuclei involved in the Th-U cycle, are gaining significantly in importance.

While it is clear that the experimental knowledge concerning the uranium-based reactors is very limited, the data on the fission of the nuclei involved in the Th-U cycle, are clearly insufficient. Moreover, the experiments for a full coverage of the data needed for the relevant nuclides in a desirable excitation-energy range are presently far beyond the technical and financial limits. However, a crucial need to invest special effort into these systems comes from the fact that they are precisely located in a region of the nuclear chart which has shown to exhibit abnormal features as compared to the regularities and trends observed in heavier actinides. This is known since the 1970's as the "thorium anomaly". Based on fission probabilities and angular anisotropies, this was attributed to the presence of a triple-humped fission barrier in the lighter actinides. Though, modern models challenge the quantitative impact of this third minimum (see the discussion in section 4.2). The lack of data and the limited predictive power of fission models lead to large uncertainties in the simulation of thorium-based reactors, in particular because they operate with fast neutrons in the range up to a few MeV, where, according to our analysis, the fission yields show a strong variation as a function of energy.

In the present work, we collect and analyze relevant empirical information in order to improve the description of the complexity of fission of light actinides. We eventually connect it with the presence of a triple-humped fission barrier, and confront it with the semi-empirical GEF code [7,8]. Finally, we

develop a dedicated theoretical model and produce the missing nuclear data by performing systematic model calculations.

2. Indications for abnormal features in the fission of light actinides

In the 1970's a tremendous effort has been invested in measuring high-accuracy fission excitation functions and fragment angular anisotropies (see e.g. Refs. [9,10,11]). Compared to heavier actinides, thorium isotopes show an odd behaviour. Due to the model-dependence of the analysis, the magnitude of the influence of the third barrier remains controversial even today as will be summarized in Section 4. In the present work, we introduce for the first time the fission fragment mass (equivalently, charge) distribution and the Total Kinetic Energy (*TKE*) as experimental signatures for the occurrence of a third barrier. As we show below, the latter can have a large quantitative impact on these observables. But this influence can also be very subtle due to the interplay with other effects. Accordingly, a proper theoretical treatment is critical for calculations of future thorium-based nuclear reactors, as well as for their safe operation.

In Figs. 1 and 2, the fission-fragment nuclear-charge (Z) distributions from thermal and $E_n \approx$ 14 MeV neutron-induced fission, respectively, are shown for a sample of actinide targets. Figure 1 reveals a clear deviation in position and shape of the Z distribution of the system ^{229}Th(n_{th},f) from the systematics of the heavier systems. The heavy peak is shifted to higher Z values, and the skewness is reversed. Note that the strong shift of the light peak is not relevant in the present discussion. It is a consequence of the variation of A and Z of the fissioning system. As Fig. 2 shows, at higher incident energy, the heavy peak of the system ^{232}Th(n_{14MeV},f) fits much better to the systematics of the heavier systems. Concerning the slight overshoot near Z=55, we remind the reader that also in fission induced by 14-MeV neutrons, there is a contribution due to multi-chance fission, where the system fissions at excitation energies (E*) close to the fission barrier. The influence of multi-chance fission can result in a complex interplay, and a careful analysis is required to avoid misinterpretation. Table 1 lists the neutron-to-proton (N/Z) ratios of the systems and illustrates that the compound nuclei corresponding to Fig. 1 have almost identical values. Thus, the striking deviation (or "anomaly") appearing at the lowest excitation energy in Fig. 1 for ^{229}Th(n_{th},f) cannot be attributed to a different neutron excess. Considering the distribution for ^{232}Th(n_{14MeV},f) of Fig. 2, and neglecting the possible influence of the different N/Z values of ^{229}Th and ^{232}Th, this anomaly seems to disappear at higher initial excitation energies.

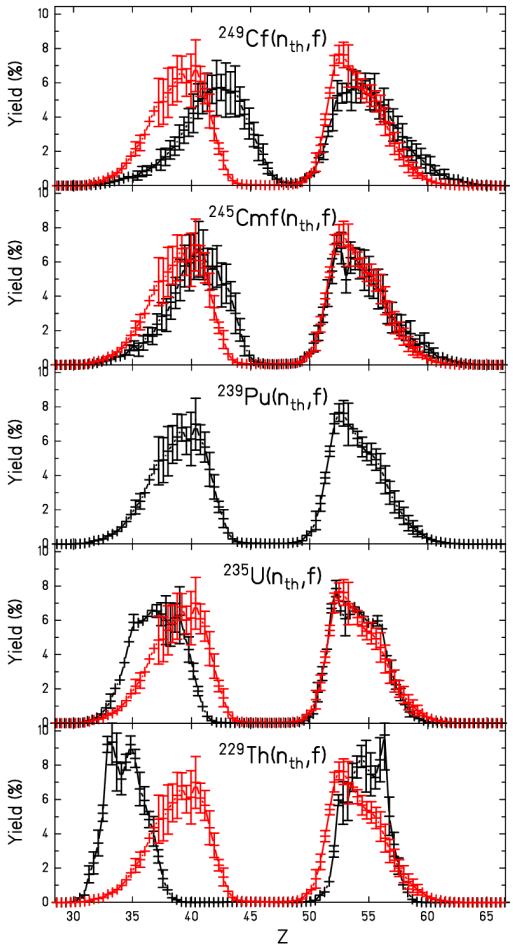

Figure 1: Nuclear-charge (*Z*) distributions of the fission fragments, formed by thermal-neutron-induced fission of a series of actinide target nuclei. The *Z* distributions were deduced from the post-neutron mass distributions of the ENDF-B/VII evaluation [3]. The charge polarization and the emission of prompt neutrons was neglected. The distribution of the system ^{239}Pu(n_{th},f) is added in red to the distributions of the other systems. The abnormal position and shape of the heavy peak of the system ^{229}Th(n_{th},f), which does not fit to the systematics of the heavier systems, is clearly seen.

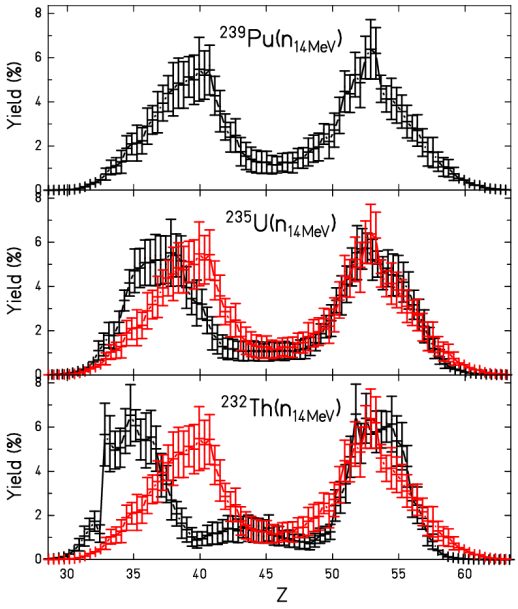

Figure 2: Nuclear-charge distributions of the fission fragments, formed by neutron-induced fission (E_n = 14 MeV), of a series of actinide target nuclei. The *Z* distributions were deduced from the post-neutron mass distributions of the ENDF-B/VII evaluation [3]. The charge polarization and the emission of prompt neutrons was neglected. Because there are no data on fission induced by 14 MeV available for ^{229}Th, the fission-fragment *Z* distribution of ^{232}Th(n_{14MeV},f) is shown. The distribution of the system ^{239}Pu(n_{14MeV},f) is added in red to the distributions of the other systems.

The *Z* distributions were chosen for this comparison, because of the leading role of the proton shells for the position of the asymmetric component in the fission of the actinides that had been deduced in a previous work [12]. For four of the systems shown in Fig. 1, there exist also direct measurements of the fission-fragment *Z* distribution (for ^{229}Th see Ref. [13] , for ^{235}U see Ref. [14], for ^{239}Pu see Ref. [15], and for ^{249}Cf see Ref. [16]). They are not shown here in the interest of a consistent and homogeneous comparison, because there exist no direct measurements for spontaneous fission and for fission induced by 14-MeV neutrons.

Nucleus	**^{230}Th**	**^{233}Th**	**^{236}U**	**^{240}Pu**	**^{246}Cm**	**^{250}Cf**
N/Z	1.555	1.589	1.565	1.553	1.563	1.551

Table 1: List of the neutron-to-proton ratios (*N/Z*) of the compound nuclei corresponding to the *Z* distributions shown in Figs. 1 and 2.

Recently, fragment distributions for fission of ^{233}Pa as induced by protons impinging on ^{232}Th were measured over a larger excitation-energy range with small energy increments [17]. They show regular

shifts in the position of the asymmetric peaks of the mass distribution at the onset of the different stages of multi-chance fission. It seems reasonable to assume that this finding is closely connected with the anomaly of the system ^{229}Th(n_{th},f), shown in figure 1. Unfortunately, this structure is not a direct signature of the fission at low excitation energies, because it is mixed with fission in previous stages of the multi-chance fission, and because the spread of the kinetic energies of the pre-fission neutrons tends to wash out the signature produced by the last-chance fission. We will get back to this difficulty and its handling within the GEF code in Section 5.

We would like to mention that the deviation of the directly measured *Z* distribution of the system ^{229}Th(n_{th},f) from the systematics of the heavier systems has already been noticed long time ago [18]. Abnormal features in mass distributions and total kinetic energy (*TKE*) have been reported, for example in bremsstrahlungs-induced fission of ^{232}Th, see Ref. 19 and references therein. Also a strong dependence of the *Z* distribution from the kinetic energy of the light fragment has been seen and attributed to the shrinking of the phase space at high *TKE* value that almost exhausts the *Q* value. In the present work, we focus on the properties of the *TKE*-integrated fission-fragment distribution and, in particular, on the dependence on the initial excitation-energy, because this is of prime importance for the technical applications considered here.

As we mentioned already, also the *TKE* at low *E** seems to be a very good signature of the suppression of compact shapes. This aspect will be discussed in detail in section 5.

3. Incomplete data basis

Since it is impossible to measure all the systems of concern for present and future applications (note that some isotopes of interest are shorted-lived, and excitation energies above the fission barrier from zero to several MeV are of interest), a reliable evaluation is required. The latter is generally based on existing measurements for a few systems. There exist also cases where missing measurements are supplemented by model predictions. Unfortunately, the accuracy achieved by current evaluations remains limited due to the lack of suited experimental data. We give a brief summary below.

Over the years, the experimental techniques improved substantially, but the determination of the yields of fission fragments with full resolution in mass *A* and atomic number *Z* still remains a challenge. Most data were obtained with radiochemical techniques for the fission induced by neutrons. Radiochemical techniques are among the few options that provide a full identification of the fragments in *A* and *Z*. However, there are several restrictions:
(i) Appropriate target material is required. The target material must be stable or long-lived.
(ii) Neutrons with high flux and well defined energy must be available. By this reason, most experiments were performed with thermalized, “fast” and 14-MeV neutrons.
(iii) The identification of the fragments by gamma radiation often requires chemical separation and transport of the sample to a background-free location. This sets a lower time limit in the order of seconds or minutes and, thus, makes it impossible to detect short-lived fragments.

Additional problems arise, because fission attributed to "thermal neutrons" often has contributions from fission at higher energies, due to incomplete thermalization of the incident neutrons. For targets that are not fissile by thermal neutrons, the data named "(n_{th},f)" have their origin in reality mainly from higher neutron energies [20]. This is true for many systems included in the official evaluations.

Also "fast neutrons" are not well defined, and their energy distribution can be large. Evaluated data listed in the category *fast-neutron-induced fission* reach from an average of 500 keV to about 2 MeV (in particular for $^{238}U(n_{fast},f)$, due to the high fission barrier) [20]. The energy is distributed over a more or less broad energy range, and the variation of the average energy from system to system hides a clear signature of the excitation-energy dependence of fission observables.

Other techniques have been developed recently, but only few provide a full identification of the fragments in *A* and *Z*, which is mandatory for the generation of suitable high-quality nuclear data. However, they suffer from other problems:
(i) Experiments at GSI, Darmstadt, measure the fragments produced in the fission of heavy, relativistic projectiles induced by electromagnetic excitation in a Pb or U target in inverse kinematics. [21,22]. The resolution in *A* and *Z* is excellent, but the excitation-energy distribution is broad and not tunable. Furthermore, the nuclei that can be studied are produced in fragmentation reactions from stable or long-lived material. Thus, their variety is limited to nuclei lighter or with a mass equal to the primary projectiles.
(ii) Experiments at GANIL, Caen, measure the fragments produced in the fission of heavy projectiles with energies slightly above the Coulomb barrier, where fission is induced by transfer reactions from light target nuclei [23], Here, again, the projectiles must be stable or long-lived, and the variety of transfer products is limited. Cuts on excitation energy with a range below a few MeV are difficult due to limited resolution and statistics.

In summary, the evaluated data on fission yields for so-called thermal, fast and 14-MeV neutrons that exist only for a handful of target nuclei lack the needed precision. In particular, high-quality direct data on the evolution of the fission yields as a function of the initial excitation energy in the technically most important range of a few MeV above the fission barrier do not exist to our knowledge. To circumvent the limitations of current evaluations, a theoretical model with high predictive power is required. In the context of modern applications, it is crucial that the selected model manages to describe the abnormal features of fission of light actinides. In this work, we propose the GEF code [7,8] as a fast and flexible approach to provide reliable fission yields, consistently from light to heavy actinides, and from the threshold to high energies.

4. Physics ideas and implementation in GEF

4.1 Framework of the GEF code

GEF is a semi-empirical model of the fission process, which is being widely used. It combines a good description of measured data due to the combination of the presence of adjustable empirical parameters with the power for extrapolations to unmeasured systems due to its theoretical backbone [7].

From the beginning, the model was very successful in describing fission observables for the heavier actinides with $Z > 92$ up to $Z=100$ and beyond. However, for lighter actinides, deviations with respect to the systematic behaviour of the heavier systems have been observed: In spontaneous fission and in thermal-neutron-induced fission for $Z \leq 92$, the dominant asymmetric component became narrower, and it was shifted towards higher asymmetry, as discussed in Section 2. In previous GEF versions, these deviations were considered by introducing purely empirical (“local”) parameters for the

concerned systems. Recently, the experiment of Berriman et al. [17], mentioned above, revealed by a comparison with GEF-Y2018/V1.1 that this empirical parametrization was insufficient. In the present work, we propose a common explanation to these deficiencies of the previous GEF versions. The ideas and the formalism implemented recently to enhance the model in this respect are detailed in the following sections. It is based on the presence of a third barrier in the potential-energy surface of light actinides evolving towards the scission-point configurations. The formalism described here is already incorporated in the most recent versions of the GEF code, starting with version 2013/V3.1, and it describes the experimental observations well.

4.2 A third barrier in the light actinides

As mentioned above, the abnormal features of the fission-fragment mass (charge) distributions of light actinides are attributed to a third barrier on the fission path. We assume that the third barrier tends to increase the potential energy near scission so much that, at low initial excitation energies, the nascent fragments under certain conditions may be hindered to reach the scission point due to lack of energy.

The peculiar behaviour of some light actinides was noticed in the 1970's based on measurements of fission excitation functions and fragment angular distributions (see Refs. [11,24,25] for representative publications on such experiments). In particular, within a statistical-model analysis assuming a double-humped fission barrier profile, the parameters extracted for $^{231\text{-}234}$Th were found to be incompatible with theoretical estimates based on the Strutinsky method (a theory, which was otherwise successful in explaining asymmetric fission of actinides). On the contrary, the parameters extracted for ^{240}Pu were seen to match theoretical predictions well.

A connection between the presence of a third minimum in the fission path, resulting in a triple-humped barrier, and the "thorium anomaly" was first made by Möller and Nix at the IAEA symposium in Vienna in 1973 [26]. A wealth of experimental information on fission probabilities and angular anisotropies were collected in a more widespread area of the actinide region in the following three decades. All confirmed the necessity to consider a triple-humped fission barrier to understand the lightest actinides at low excitation energy (see e.g. Refs. [27,28,29,30,31,32]). As a general rule, the depth of the third minimum required by the statistical-model calculations of these works was rather shallow, in accordance with the early predictions by Möller [33]. In the 1990's, new calculations by Cwiok et al. [34] predicted, however, deep third minima. While some subsequent experiments, see e.g. Ref. [35], confirmed the calculations of Cwiok et al., other, e.g. Ref. [36], did not, re-starting the debate about the magnitude of the third potential well. In this context, Kowal et al. [37] recently pointed to a flaw in the calculations of Ref. [36], and corroborated the shallowness of the third minimum obtained in the pioneering predictions [26,33]. That led to a resurgence of interest, and new calculations within most modern models were done over the past decade [38,39,40,41,42]. Independently of the approach, the macroscopic-microscopic or the self-consistent, all results predict a shallow third minimum in the lighter actinides, typically between thorium and uranium, and which vanishes with increasing neutron number.

All studies on the shape of the fission barrier, and, in particular, on the occurrence of a third minimum, rely on fission excitation functions and angular anisotropies. The analysis and interpretation are based on statistical-model calculations, with typically 5 to 10 parameters. The extracted barrier profile therefore suffers from a considerable uncertainty due to large model-dependence, which may have

contributed to the aforementioned debate. Additional signatures are highly desirable. To the best of our knowledge, no investigation of the specific impact of the third minimum on the fission fragment mass (charge) and *TKE* distributions, and their evolution with excitation energy, was performed prior to this work. As the present study shows, these quantities are subtle signatures of the last stage of the barrier profile, as will be discussed in section 4.4.

4.3 Updated formalism used in GEF

The following section describes the technical aspects of the formalism implemented in the GEF code that accounts for the effects attributed to the third barrier. The physical arguments for these changes will be given in section 4.4.

4.3.1 Variation of the shape of the S2 peak

The original aim of GEF was to calculate the distributions of the different observables (for example mass distributions) by considering the populations of levels in a potential pocket representing a given fission valley associated with a certain fission channel. This is a rather customary procedure in the domain of (semi-)empirical models of fission, and it has proven to be successful. In the GEF code, assuming that the potential is parabolic, the population of levels is given by that of an harmonic oscillator, and the resulting mass distribution is therefore a Gaussian. While this was found to work well for the standard 1 (S1) and super-asymmetric (SA) channels, for the standard 2 (S2) channel, however, the observed mass (charge) distributions showed deviations from a Gaussian. To account for this special feature of S2, an empirical modification was introduced in GEF, involving the multiplication of the Gaussian with an additional shape function. In practice, the shape of the mass distribution was modified by convoluting the Gaussian of a (simplified) parabolic potential pocket with a "box" (rectangular distribution), see Ref. [7] for details.

The key parameter that is expected to govern the influence of the postulated third barrier is assumed to be the intrinsic excitation energy available at the third barrier. Unfortunately, there is no direct experimental information available on this quantity. It is estimated here by use of quantities that are closely related to empirical observations. This method is rather approximate, but it is expected to reproduce the major trends.

The height of the third barrier (E_c) is deduced from the semi-empirical systematics of the first and the second barrier (E_a and E_b) used in the GEF code by a linear extrapolation:

$$E_c = E_b + (E_b - E_a) \quad (1)$$

The available energy above the third barrier is given by:

$$E_c^{intr} = E_{gs}^{intr} - E_c \quad (2)$$

E_{gs}^{intr} is the initial excitation energy of the fissioning nucleus above the ground state.

In the GEF code, the mass distribution of the S2 fission channel is given by the convolution of a Gaussian with a rectangular distribution, as discussed above. To account for a third barrier, the shape variation of the heavy peak of the S2 fission channel is expressed by a multiplication with the following linear function:

$$F_{corr} = (A - A_c) / L_{box} * R_{slope} * R_{norm} \quad (3)$$

A_c is the mean value of the mass distribution in the heavy S2 peak. Negative values of F_{corr} are set to zero, while R_{norm} keeps the integral of the S2 peak. L_{box} is the size of the rectangular box that is used for the description of the mass peak of the S2 channel.

The formula that determines the slope is:

$$R_{slope} = \exp(-E^{intr}_{c,mod} * \exp(2.6 * (S_n - S_p))) \quad (4)$$

We found that the data of Fig. 6 are better reproduced, when the term E^{intr}_c , defined in equation (2), is replaced by

$$E^{intr}_{c,mod} = E^{intr}_c + E^{diss} - \Delta E \ . \quad (5)$$

E^{diss} is the dissipated energy present at scission that is used in GEF, and $\Delta E = 3$ MeV is a constant adjustable parameter. The values of these two quantities are rather close [7]. Thus, they nearly cancel. However, this modification introduces a dependence on the dissipation that seems to be present in the data. The quantity E^{diss} is rather well determined by the odd-even effect in fission-fragment Z distributions. Note that different approaches obtain rather similar relations between the excitation energy at scission and the magnitude of the odd-even effect, see Refs. [43,44,45].

For a good agreement with the data, it was necessary to add an empirical term with (S_n-S_p), the difference between the separation energies of neutrons and protons of the fissioning nucleus, in order to account for an apparent influence of the neutron excess.

The parameters characterizing a few systems are given in Tables 2 and 3.

System	E_a **(MeV)**	E_b **(MeV)**	E_b-E_a **(MeV)**	E^{intr}_{sci} **(MeV)**	$E^{intr}_{c,mod}$ **(MeV)**	S_n **(MeV)**	S_p **(MeV)**	S_n-S_p **(MeV)**	**Slope**
Th229T	5.70	6.09	0.39	1.53	- 1.86	6.02	5.84	0.18	3.5
U233T	5.69	5.57	-0.12	3.72	+ 0.84	6.18	5.35	0.82	1.79
U235T	5.76	5.73	-0.026	2.53	- 0.45	5.93	5.77	0.16	0.54
Pu239T	5.70	5.09	-0.61	4.87	+ 2.48	6.08	5.28	0.80	0.24
Pu241T	5.61	5.10	-0.50	4.10	+ 1.61	5.84	5.69	0.15	0.068
Cm247T	6.07	4.96	-1.11	4.02	+ 3.84	5.87	5.40	0.47	0.026

System	E_a (MeV)	E_b (MeV)	E_b-E_a (MeV)	E_{sci}^{intr} (MeV)	$E_{c,mod}^{intr}$ (MeV)	S_n (MeV)	S_p (MeV)	S_n-S_p (MeV)	Slope
Cf249T	6.02	4.08	-1.94	9.07	+ 8.01	6.15	4.74	1.41	0.0083

Table 2: Characteristic parameters for a few systems with long-lived target nuclei that enter into the description of the shape variation of the mass peak of the S2 component.
Note: Th229T indicates the reaction ^{229}Th(n_{th},f), and so on. E_a and E_b are the heights of the first, respectively, second barrier used in GEF, see [7] . E_{sci}^{intr} is the intrinsic excitation energy at scission, used in GEF, see [7]. $E_{c,mod}^{intr}$ is the schematic estimation of the intrinsic excitation energy at the third barrier given by equation (5). The separation energies are taken from Ref. [46]

Neutron energy (MeV)	$E_{c,mod}^{intr}$ (MeV)	Slope
0.5	- 1.15	2.85
1	- 0.45	2.36
1.5	+ 0.08	1.48
2	+ 0.57	0.90
5	+ 3.56	0.045

Table 3: Evolution of the characteristic parameters that determine the shape of the S2 mass peak for incident neutrons with different kinetic energies for the system ^{229}Th(n,f).

4.3.2 Suppression of the S1 and the SA fission channel

In addition to the shift of the mean value and the complex shape of the S2 peak (in *A* and/or *Z*), there is an additional deviation that can be deduced from the *Z* distributions shown in figure 1, namely the suppression of the S1 fission channel. The suppression of S1 has a sizable influence on the shape and the position of the asymmetric peak (in *A* and/or *Z*). The yield of SA is, on the contrary, very small for the nuclei of interest so that it is hardly observable [47]. However, we also introduced a suppression of the super-asymmetric fission channel in GEF in order to obtain agreement with the measured yields in the tails of the mass distributions at large asymmetry, see below.

The corrected yields for S1, Y_{corr}(S1), and SA, Y_{corr}(SA), respectively, are given by:

$$Y_{corr}(S1) = Y(S1) * 1/(1+\exp(4*(E_b - E_a) - E_b^{intr} - E_{diss} + \Delta E)) \quad (6)$$

$$Y_{corr}(SA) = Y(SA) * 1/(1+\exp(4*(E_b - E_a) - E_b^{intr} - E_{diss} + \Delta E)) \quad (7)$$

with $E_b^{intr} = E_{gs}^{intr} - E_b$ (8)

Equations (6) and (7) resemble the equations for the transmission through a potential barrier of an inverted parabola. The factor of 4 and the energy shift ΔE = + 3 MeV are the two adjusted parameters in these equations.

The calculations of this work have been performed with GEF-Y2023/V3.2. As we demonstrate in Section 5, the approach works well. That is, the observed deviations in the observables can be understood by a suppression of very compact and of very elongated configurations at scission, leading to a reduction of the S1 and the SA fission channels, as well as to a concentration on the more asymmetric side of the S2 channel. Since the yield of the SA channel is very small in the fission of light actinides, the suppression of very elongated shapes at their fission is deduced from GEF calculations. While GEF reproduces well the mass distribution for spontaneous fission of ^{252}Cf with a yield of 7.2 % for SA and the mass distribution of ^{239}Pu(n_{th},f) with a yield of 1 %, a suppression by a factor of 5 is necessary to reproduce the measured mass distribution of ^{235}U(n_{th},f) in the far asymmetric wings with a yield of 0.3 % in the SA channel.

We may thus conclude that in lighter actinides, fission paths with extremely compact and extremely elongated configurations are suppressed for low excitation energies at freeze-out. Note that the freeze-out is defined as the moment, when the final mass and/or Z distribution of the fission fragments is defined. This happens, before the scission configuration is reached, due to the influence of inertia and friction on the collective dynamics. See also the following section 4.4. All these effects are attributed to the influence of the third barrier.

4.4 On the topology and the dynamics around the third barrier

GEF is based on the assumption that the fragment shells are present to a high degree at the second barrier [48]. This imposes that the fragment shells are also dominant at the third barrier. It is not consistent, if we assume other, different, potential valleys at the third barrier. However, this argument still allows for systematic changes of the macroscopic potential. For example, the curvature of the macroscopic potential against mass-asymmetric distortions and against more or less elongated configurations may vary [49]. The observations of the suppression of very compact and, possibly, very elongated shapes may be explained that way.

Concerning the dynamics, two effects are expected: (i) Because the valleys of the different fission channels should be present consistently from the second barrier until scission, the flux captured in one valley should not be able to leave it. Still, the shape of the fissioning nucleus may be modified by shifting to one or the other side of the valley in terms of the mass-asymmetry degree of freedom by the modified macroscopic potential. (ii) The excitation energy of the fissioning nucleus might fall below the potential energy that is needed to pass the third barrier and to reach the scission configuraton. In that case, fission is forbidden and the flux will return back to the second minimum or start again towards fission in another valley. These ideas are based on the picture of individual trajectories of the system in the multi-dimensional deformation space by the solution of the Langevin equations. It explains both the change of the shape of the mass distribution of S2, and the suppression of a specific fission channel. Due to the different character of the dynamics of (i) and (ii), the functions that describe the two possibilities, need to be somewhat different. This may be the explanation for the absence of an (S_n-S_p) dependence of the yield suppression of S1 and SA. A more detailed discussion of this physics will be the topic of a dedicated publication [50].

4.5 Evolution of abnormal features with excitation energy

The deviation seen in the fission of light actinides from the systematic behaviour of the heavier actinides appears only at low excitation energies E^* and disappears already by increasing E^* by a few MeV, as illustrated in Figs 1 and 2. This gives rise to a drastic variation of the fission-fragment yields as a function of excitation energy, and, in particular, at energies close to the fission barrier. In this sense, it behaves in a similar way as the odd-even effect in the fission-fragment Z distributions [51], although the physics behind is different. While the fragility of pairing effects in fission against modest thermal excitations is well known, shell effects usually survive up to excitation energies in the order of 10 to 20 MeV. Thus, the fast disappearance of the suppression effect is a priori unexpected. The above detailed formalism permits to naturally take the evolution with E^* into account in GEF.

5. Benchmark

The measured fission yields of ^{229}Th(n_{th},f), ^{233}U(n_{th},f), ^{235}U(n_{th},f), and ^{238}U(spont.fission) gave us the impetus for the idea of the suppression of very compact and very elongated configurations at scissions, introduced in this work, and for the development of its quantitative description in GEF. The parameters appearing in the enhanced GEF formalism were determined by a fit to these data. The measured mass distributions are compared with GEF calculation with and without the suppression effect in figure 3, demonstrating the capability of the updated code to describe the abnormal features discussed previously.

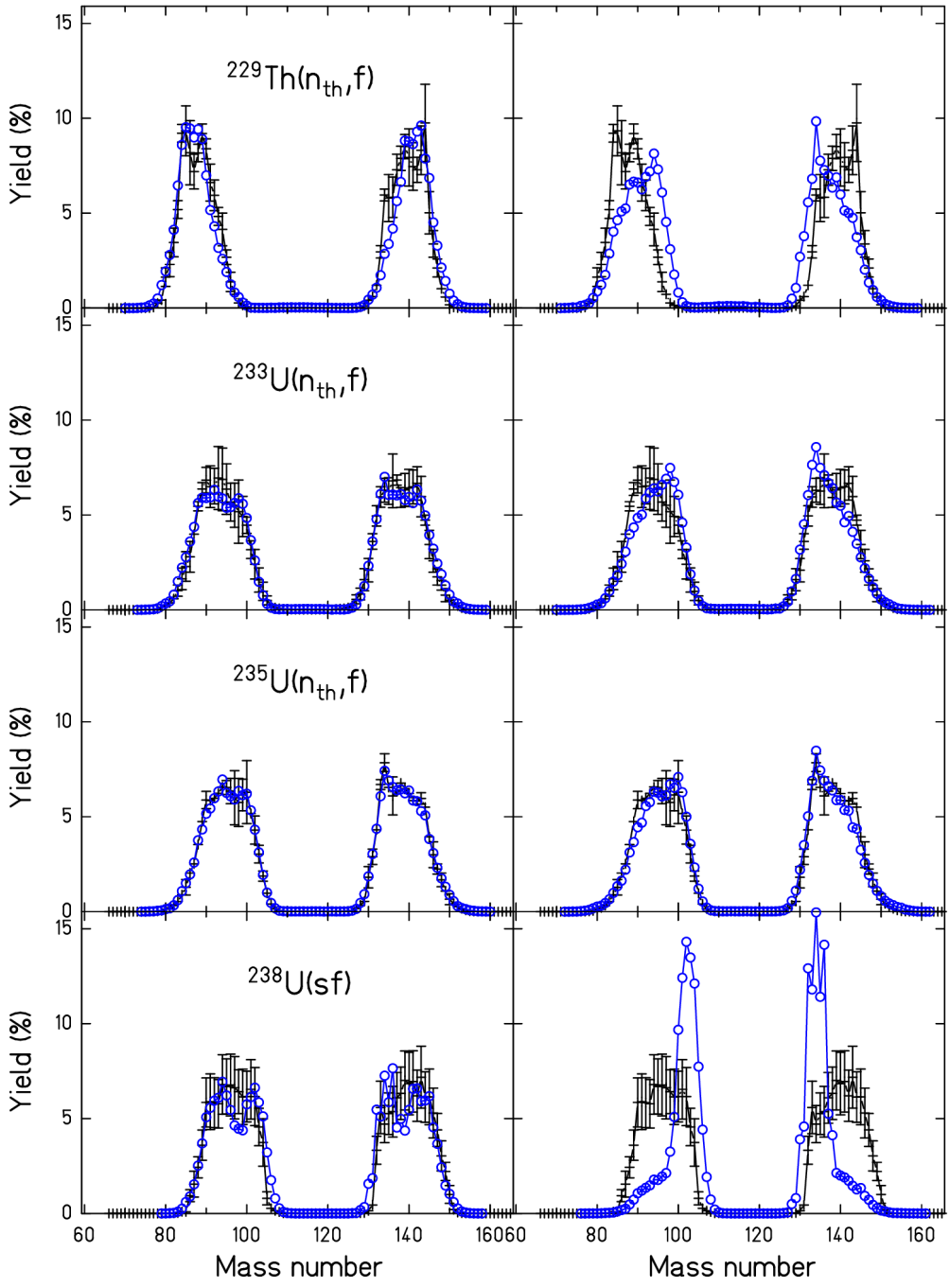

Figure 3: Empirical fission-fragment mass distributions [3] of four key systems (black symbols and error bars) that reveal the suppression effect that is attributed to the influence of a third barrier in this work are compared with GEF calculations (blue circles) with (left part) and without (right part) the suppression effect.

The suppression of compact shapes and its interplay with multi-chance fission is seen in the data on the fission of ^{233}Pa by Berriman et al. [17]. Figure 4 shows the mean mass of the light fragment (defined by the left half of the full mass distribution) from GEF as a function of the incident proton energy. Similar to experiment [17], the calculation exhibits very clear structures. The change of slope at E_p = 7, 13, 21 MeV is caused by the onset of the successive fission chances, which imply an abrupt decrease of the excitation energy of the residual system. This decline leads to a suppression of compact shapes in the population of the favored heavy fragment, which means that its mean mass increases. Accordingly, the mean mass of the light fragment decreases. This contribution of a portion of low-energy fission above the threshold for different stages of multi-chance fission is clearly seen by the regions with negative slope (positive slope in Fig. 8c of [17], where the heavy fragment is considered). The overall trend of the mean light mass to increase in Fig. 4 is due to the increasing contribution of the symmetric fission channel with increasing incident-proton energy. The calculation of Fig. 4 is at least qualitatively compatible with the experimental results of Berriman et al. [17]. Unfortunately, a quantitative comparison is hampered by the analysis procedure used in Ref. [17]: The mean mass of the heavy fragment was evaluated there from a local (Gaussian) fit around the maximum of the peak. Symmetric fission, therefore, does not contribute, but the extracted value depends somehow on the range of the fit and on the mass resolution of the experiment. A more quantitative comparison is postponed to a forthcoming publication [50].

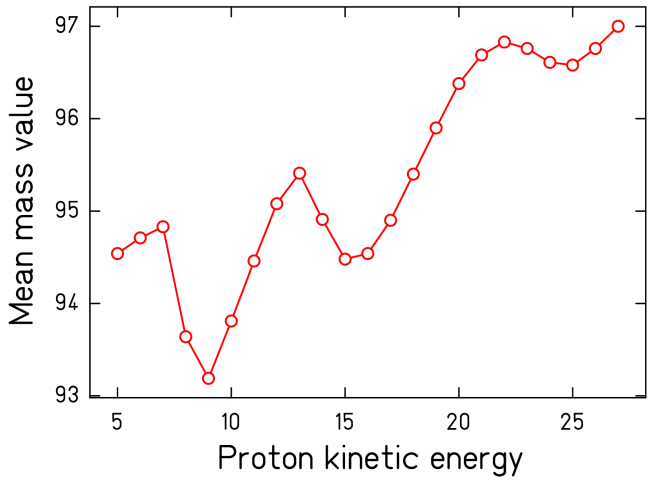

Figure 4: The symbols show the result of GEF calculations for the mean value of the light part ($A \leq 116$) of the mass distribution from the reaction ^{232}Th(p,f) as a function of the incident-proton energy. The line is drawn to guide the eye. The downward kinks appear at the thresholds of higher-chance fission contributions (E_p = 7, 13, 21 MeV). The global slope is mainly caused by the increasing yield of the symmetric fission channel.

The influence of the suppression of compact and very elongated shapes on the *TKE* observable is finally shown in Fig. 5 for neutron-induced fission of ^{238}U. ^{238}U, as a non-fissile nucleus by thermal neutrons, is particularly well suited to show the effect, which appears most strongly at energies close to the fission barrier, because states in the vicinity, and even below the barrier can be populated with incident low-energetic neutrons. The difference between the two calculations below E^* = 8 MeV illustrates the energy dependence of the suppression effect, which is implemented in the updated GEF

code. Although the absence of experimental data below E^* = 6.2 MeV (E_n = 1.4 MeV) prevents us to study the slope of the decrease in detail; the beginning of the decline is clearly shown in the data.

Note that the low *TKE* value of 169 MeV for spontaneous fission (E^* = 0) of ^{239}U obtained by GEF is consistent with the low yield of the S1 fission channel in the measured mass distribution of the spontaneous fission of ^{238}U, see Fig. 3. (The mass distributions of the two neighbouring isotopes may be assumed to be very similar.) This "bridge" between the mass distribution and the *TKE* confirms nicely the idea of the suppression of very compact configurations by the third fission barrier. The suppression of very elongated shapes, mentioned above, does not have a sizable effect on the TKE due to the low yield of the super-asymmetric fission channel in the light actinides.

Figure 5 shows that the *TKE* is a very sensitive, and particularly subtle, signature of the presence and the fading out of the suppression effect. This effect counteracts the negative slope above $E^* \approx 7$ MeV, which is caused by the decreasing yield of the S1 fission channel above E_n = 2 MeV and the increasing yield of the symmetric fission channel.

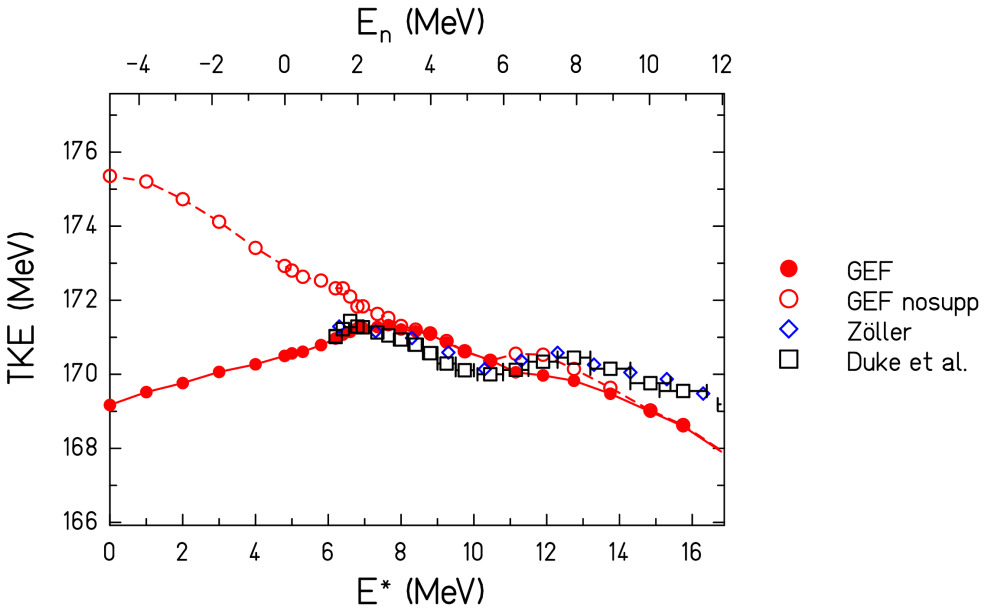

Figure 5: Pre-neutron total kinetic energy of the fission fragments from the reaction ^{238}U(n,f) as a function of the incident-neutron energy (upper scale) and the excitation energy (lower scale). The measured data [52,53] are compared with the results of the GEF code with and without the application of the suppression of very compact and very elongated configurations. The lines are drawn to guide the eye. The horizontal error bars correspond to the widths of the incident-neutron energy ranges of the data from Ref. [53]. The GEF results have been shifted by -0.3 MeV to be better comparable with the data. (The range of fictive negative E_n values is added to show the behaviour in an extended excitation-energy range.)

6. Quantitative predictions

The new feature presented in this work has important impact on the planning and on the operation of modern and future power plants, in particular the Th-U fuel cycle, where fission occurs at variable energies, from threshold up to typically a few MeV above the fission barrier. ^{233}Pa is a key isotope for Th-U fuel cycle. Its importance in the operation of nuclear facilities like fission reactors or accelerator-driven systems connects with two aspects (known as a “protactinium effect”): First, decrease of the reactivity of the reactor due to capture of neutrons and, second, increase of the reactivity after reactor stop due to inventory transformation of ^{233}Pa into ^{233}U via β-decay. Any knowledge on the fission properties of ^{233}Pa is thus essential.

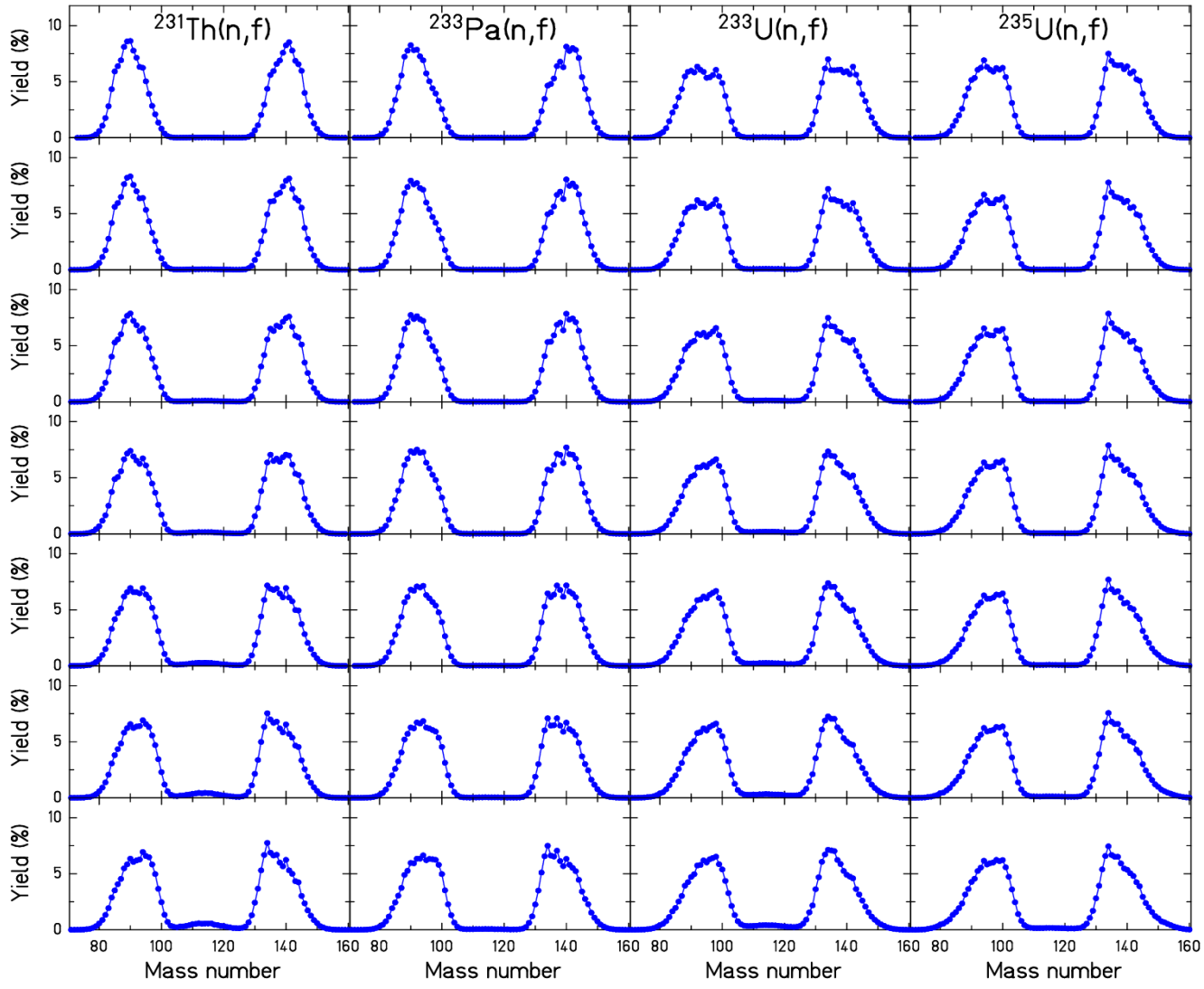

Figure 6: Illustration of the suppression effect on the fission-fragment mass distributions after prompt-neutron emission for neutron-induced fission of several target nuclei (^{231}Th, ^{233}Pa, ^{233}U, ^{235}U). The results of GEF-Y2023/V3.2 are shown for incident-neutron energies from thermal to 3 MeV in increments of 0.5 MeV from top to bottom.

To our knowledge, the GEF code is the only tool that is able to reproduce the observed abnormal features and to estimate the effect on (nearly) all fission observables for all nuclei in the light actinides as well as the variation with excitation energy. The GEF code is available in the internet [54,55,56].

The fission yields from neutron-induced fission of 144 target nuclides with $86 \leq Z \leq 98$ and incident neutron energies between thermal and 30 MeV have been calculated, and they are made available to the community [57,58]. These GEFY data tables are also distributed by the NEA via the JANIS software [59]. The mass distributions for a few representative systems with technical relevance are presented in Fig. 6.

7. Conclusion

In this work, complex and abnormal features in the yields from the fission of light actinides at low excitation energies are investigated. We revisited previously noticed deviations of the yields in thermal-neutron-induced fission from the monotonous trend that is observed for heavier systems. We widened the analysis to higher excitation energies, and, by the use of recent data, to structures appearing in multi-chance fission as well as to a pronounced drop in the total kinetic energies.

These complex features were attributed to the influence of a third minimum, respectively barrier, in these nuclei, and, based on this idea, we have developed a model description and recently implemented it in the GEF code. The enhanced modeling successfully grasps the complexity of light actinides by reproducing properly their critical impact on the earlier mass-yield measurements, as well as on other fission observables, and, in particular, on the total kinetic energy, which was not addressed in the past. The GEF code finally offers a consistent description over the entire region of actinides. It is used to provide systematic predictions on fission yields, and in this work, more specifically where the abnormal features appear. This concerns nuclei involved in the Th-U fuel cycle but also all uranium isotopes that are present in conventional fission reactors. Thus, the results of the present study are highly relevant for the design and the operation of conventional and future reactors.

Acknowledgement

We thank K. Mazurek, P. Möller, K. Pomorski for enlightening discussions. The work was supported by the French-German collaboration between IN2P3-DSM/CEA and GSI, under Agreement No. 19-80.

1 “Nachweis der Entstehung aktiver Bariumisotope aus Uran und Thorium durch Neutronen-Bestrahlung: Nachweis weiterer aktiver Bruchstuecke bei der Uranspaltung"
Otto Hahn, Fritz Strassmann, Naturwissenschaften 27 (1939) 89

2 “Nuclear science for the Manhattan Project and comparison to today’s ENDF data.”, *M. B. Chadwick,* Nucl .Technol. (2021) 207: S24–61. doi:10.1080/00295450.2021.1901002

3 “ENDF/B-VII.1 nuclear data for science and technology: cross sections, covariances, fission product yields and decay data”, *M. B. Chadwick, M. Herman, P. Oblozinsky, M. E. Dunn, Y. Danon, A. C. Kahler, D. L. Smith, B. Pritychenko, G. Arbanas, R. Arcilla, R. Brewer, D. A. Brown, R. Capote, A. D. Carlson, Y. S. Cho, H. Derrien, K. Guber, G. M. Hale, S. Hoblit, S. Holloway, T. D. Johnson, T. Kawano, B. C. Kiedrowski, H. Kim, S. Kunieda, N. M. Larson, L. Leal, J. P. Lestone, R. C. Little, E. A. McCutchan, R. E. MacFarlane, M. MacInnes, C. M. Mattoon, R. D. McKnight, S. F. Mughabghab, G. P. A. Nobre, G. Palmiotti, A. Palumbo, M. T. Pigni, V. G. Pronyaev, R. O. Sayer, A. A. Sonzogni, N. C. Summers, P. Talou, I. J. Thompson, A. Trkov, R. L. Vogt, S. C. van der Marck, A. Wallner, M. C. White, D. Wiarda, P. G. Young,* Nucl. Data Sheets 112 (2011) 2887

4 “An overview of thorium as a prospective natural resource for future energy“, *R. K. Jyothi, L. G. Tumajan Costa De Melo, R. M. Santos, Ho-Sung Yoon,* Front. En. Res. 11 (2023) 1

5 "Closed U-Pu and Th-U cycle in sixteen selected reactors: Comparison of major equilibrium features", *J. Krepel, E. Losa*, Ann. Nucl. En. 128 (2019) 341

6 “Thorium’s Long-Term Potential in Nuclear Energy”, *Artem Vlasov,* IAEA Bulletin, vol. 64-3, Sept. 2023

7 "General description of fission observables: GEF model code"**,** *K.-H. Schmidt, B. Jurado, C. Amouroux, C. Schmitt, Nucl. Data Sheets 131 (2016) 107*

8 "Extensive study of the quality of fission yields from experiment, evaluation and GEF for antineutrino studies and applications", *K.-H. Schmidt, M. Estienne, M. Fallot, S. Cormon, A. Cucoanes, T. Shiba, B. Jurado, K. Kern, Ch. Schmitt,* Nucl. Data Sheets 173 (2021) 54

9 "Subbarrier fission resonances in Th isotopes", *B. B. Back, H. C. Britt, J. D. Garrett, Ole Hansen* Phys. Rev. Lett. 28 (1972) 1707

10 "Fission of double even actinide nuclei induced by direct reactions", *B. B. Back, Ole Hansen, H. C. Britt, J. D. Garret,* Phys. Rev. C 9 (1974) 1924

11 “Nuclear spectroscopy of highly deformed ^{231}Th”, *G. D. James, J. E. Lynn, L. G. Earwaker*, Nucl. Phys. A 189 (1972) 225

12 "Nuclear-fission studies with relativistic secondary beams: analysis of fission channels"
C. Böckstiegel, S. Steinhäuser, K.-H. Schmidt, H.-G. Clerc, A. Grewe, A. Heinz, M. de Jong, A. R. Junghans, J. Müller, B. Voss, Nucl. Phys. A 802 (2008) 12-25

13 "Characteristics of mass and nuclear charge distributions of ^{229}Th(n_{th},f). Implications for fission dynamic", *J. P. Bocquet, R. Brissot, H. R. Faust, M. Fowler, J. Wilhelmy, M. Asghar, M. Djebara*
Z. Phys. A 335 (1990) 41

14 "Nuclear charge and mass yields for $^{235}U(n_{th},f)$ as a function of the kinetic energy of the fission products", *W. Lang, H.-G. Clerc, H. Wohlfarth, H. Schrader, K.-H. Schmidt*
Nucl. Phys. A 345 (1980) 34

15 "Fission yields at different fission-product kinetic energies for the thermal-neutron-induced fission of ^{239}Pu" *C. Schmitt, A. Guessous, J. P. Bocquet, H.-G. Clerc, R. Brissot, D. Engelhardt, H. R. Faust, F. Gönnenwein, M. Mutterer, H. Nifenecker, J. Pannicke, Ch. Ristori, J. P. Theobald*
Nucl. Phys. A 430 (1984) 21

16 "Mass, charge and energy distributions in the very asymmetric fission of ^{249}Cf induced by thermal neutrons" *R. Hentzschel, H. R. Faust, H. O. Denschlag, B. D. Wilkins, J. Gindler*
Nucl. Phys. A 571 (1994) 427

17 "Energy dependence of p + ^{232}Th fission mass distributions: Mass-asymmetric standard I and standard II modes, and multichance fission", *A. C. Berriman, D. J. Hinde, D. Y. Jeung, M. Dasgupta, H. Haba, T. Tanaka, K. Banerjee, T. Banerjee, L. T. Bezzina, J. Buete, K. J. Cook, S. Parker-Steele, C. Sengupta, C. Simenel, E. C. Simpson, M. A. Stoyer, B. M. A. Swinton-Bland, E. Williams,* Phys. Rev. C 105 (2022) 064614

18 *F. Gönnenwein, in:* C. Wagemans (Editor): The Nuclear Fission Process, (CRC Press, Boca Raton

19 "Mass and kinetic energy distributions for the photofission of ^{232}Th with 6.44 to 13.15 MeV bremsstrahlung", *M. Piessens, E. Jacobs, S. Pomme, D. De Frenne,* Nucl. Phys. A 556 (1993) 88

20 "Assessment of fission product yields data needs in nuclear reactor applications"
Kilian Kern, Maarten Becker, Cornelis Broeders
PHYSOR Advances in Reactor Physics (2012) 1

21 "Relativistic radioactive beams: A new access to nuclear-fission studies"
K.-H. Schmidt, S. Steinhäuser, C. Böckstiegel, A. Grewe, A. Heinz, A. R. Junghans, J. Benlliure, H.-G. Clerc, M. de Jong, J. Müller, M. Pfützner, B. Voss
Nucl. Phys. A 665 (2000) 221

22 "Studies of fission with ALADIN", *J.-F. Martin et al.,* Eur. Phys. J. A 51 (2015) 174

23 "Isotopic yield distributions of transfer- and fusion-induced fission from $^{238}U+^{12}C$ reactions in inverse kinematics", *M. Caamano et al.,* Phys. Rev. C 88 (2013) 024605

24 "Subbarrier fission resonances in Th isotopes", *B. B. Back, H. C. Britt, J. D. Garrett, Ole Hansen*
Phys. Rev. Lett. 28 (1972) 1707

25 "Fission of double even actinide nuclei induced by direct reactions", *B. B. Back, Ole Hansen, H. C. Britt, J. D. Garret,* Phys. Rev. C 9 (1974) 1924

26 *P. Möller and J. R. Nix,* Proceedings of the Third International Atomic Energy Agency Symposium on Physics and Chemistry of fission, 1973 (Vienna), vol. 1, p. 103.

27 "On the existence of triple-humped fission barriers in ^{231,233}Th", *J. Blons, C. Mazur, D. Paya, M. Ribrag, H. Weigmann,* Nucl. Phys. A 414 (1984) 1

28 "A third minimum in the fission barrier", *J. Blons,* Nucl. Phys. A 502 (1989) 121c

29 "Fission fragment angular distributions for neutron fission of ^{232}Th and their interpretation with a triple-humped fission barrier", *J. Caruana, J. W. Boldeman, R. L. Walsh,* Nucl. Phys. A 285 (1977) 205

30 *A. Krasznahorkay et al.*, APH N.S., Heavy Ion Physics 7 (1998) 35

31 "Study of the ^{232}Th fission barrier by electron-induced fission", *M.-L. Yoneama, E. Jacobs, J. D. T. Arruda-Neto, B. S. Bhandari, D. De Frenne, S. Pomme, K. Persyn, K. Govaert,* Nucl. Phys. A 604

32 "Subthreshold photofission of ^{235}U and ^{232}Th, *C. D. Bowman, I. G. Schröder, K. C. Duvall, C. E. Dick,* Phys. Rev. C 17 (1978) 1086

33 "Odd-multipole shape distortions and the fission barriers of elements in the region 85 <= Z <= 120", *P. Möller,* Nucl. Phys. A 192 (1972) 529

34 "Hyperdeformation and clustering in the actinide nuclei", *S. Cwiok, W. Nazarewicz, J. X. Saladin, W. Plociennik, A. Johnson,* Phys. Lett. B 322 (1994) 304

35 "Hyperdeformed sub-barrier fission resonances observed in ^{232}U"**,** *L. Csige, M. Csatlos, T. Faestermann, Z. Gacsi, J. Gulyas, D. Habs, R. Hertenberger, A. Krasznahorkay, R. Lutter, H. J. Maier, P. G. Thirolf, H.-F. Wirth,* Phys. Rev. C 80 (2009) 011301 (R)

36 "Transmission resonance spectroscopy in the third minimum of ^{232}Pa", *L. Csige, M. Csatlós, T. Faestermann, J. Gulyás, D. Habs, R. Hertenberger, M. Hunyadi, A. Krasznahorkay, H. J. Maier, P. G. Thirolf, H.-F. Wirth,* Phys. Rev. C 85 (2012) 054306

37 "Examination of the existence of third, hyperdeformed minima in actinide nuclei", *M. Kowal, J. Skalski,* Phys. Rev. C 85 (2012) 061302(R)

38 "Character and prevalence of third minima in actinide fission barriers" *Takatoshi Ichikawa, Peter Moeller, Arnold J. Sierk,* Phys. Rev. C 87 (2013) 054326

39 "Third minima in thorium and uranium isotopes in a self-consistent theory", *J. D. McDonnell, W. Nazarewicz, J. A. Sheikh,* Phys. Rev. C 87 (2013) 054327

40 "Performance of the Fourier shape parametrization for the fission process" ,*C. Schmitt, K. Pomorski, B. Nerlo-Pomorska, J. Bartel,* Phys. Rev. C 95 (2017) 034612

41 "Fission barriers of heavy nuclei within a microscopic approach", *L. Bonneau, P. Quentin, D. Samsoen* ,Eur. Phys. J. A 21 (2004) 391

42 “Cassini-oval description of the multidimensional potential energy surface for ^{236}U: Role of octupole deformation and calculation of the most probable fission path”,
K. Okada, T. Wada, R. Capote, N. Carjan, Phys. Rev C 107 (2023) 034608

43 "A combinatorial analysis of pair breaking in fission"
H. Nifenecker, G. Mariolopoulos, J. P. Bocquet, R. Brissot, Mme Ch. Hamelin, J. Crancon, Ch. Ristori
Z. Phys. A 308 (1982) 39

44 "Pair breaking and even-odd structure in fission-fragment yields", *F. Rejmund, A. V. Ignatyuk, A. R. Junghans, K.-H. Schmidt,* Nucl. Phys. A 678 (2000) 215

45 "Influence of complete energy sorting on the characteristics of the odd-even effect in fission-fragment element distributions", *Beatriz Jurado, Karl-Heinz Schmidt,* J. Phys. G: Nucl. Part. Phys. 42 (2015) 055101

46 "The AME 2020 atomic mass evaluation (II). Tables, graphs and references"
Meng Wang et al., Chinese Phys. C 45 (2021) 030003

47 "Nuclear scission", *U. Brosa, S. Grossmann, A. Müller,* Phys. Rep. 197 (1990) 167

48 "Fragment-shell influences in nuclear fission", *U. Mosel, H. W. Schmitt*, Phys. Rev. C 4 (1971) 2185

49 "Features of mass distributions of hot rotating nuclei"**,** *A. Ya. Rusanov, M. G. Itkis, V. N. Okolovich*, Phys. Atom. Nuclei 60 (1997) 683

50 *K.-H. Schmidt et al.*, in preparation

51 "Excitation energy dependence of fragment characteristics for the photofission of ^{232}Th",
K. Persyn, E. Jacobs, S. Pommé, D. De Frenne, K. Govaert, M. L. Yoneama
Nucl. Phys. A 620 (1997) 171

52 *P. Zöller,* PhD thesis, Technische Hochschule Darmstadt, Germany (1995)

53 "Fission-fragment properties in ^{238}U(n,f) between 1 and 30 MeV"
D. L. Duke, F. Tovesson, A. B. Laptev, S. Mosby, F.-J. Hambsch, T. Brys, M. Vidali
Phys. Rev. C 94 (2016) 054604

54 *https://www.lp2ib.in2p3.fr/nucleaire/nex/gef/*

55 *https://www.khschmidts-nuclear-web.eu/GEF.html*

56 *https://www.oecd-nea.org/tools/abstract/list*

57 *https://www.lp2ib.in2p3.fr/nucleaire/nex/gefy/*

58*https://www.khschmidts-nuclear-web.eu/GEFY.html*

59 *https://www.oecd-nea.org/janisweb/*